Sigma Journal of Engineering and Natural Sciences
Web page info: https://sigma.yildiz.edu.tr
DOI: 10.14744/sigma.2025.1922

Research Article

Computational fracture analysis of 3Y-TZP dental ceramics with low Al_2O_3 using peridynamics

Alireza MORADKHANI[1], Mohammad HOSEINPOUR GOLLO[1,*]

[1]*Department of Mechanical Engineering, Shahid Rajaee Teacher Training University, Tehran, 1678815811, Iran*

ARTICLE INFO

Article history
Received: 03 February 2025
Revised: 28 April 2025
Accepted: 19 May 2025

Keywords:
3Y-TZP + x wt% Al_2O_3; Dental Ceramics; Dynamic Fracture; Peridynamics

ABSTRACT

This study investigated crack growth and total energy of the system in 3 mol% yttria-stabilized tetragonal zirconia polycrystal (3Y-TZP) dental ceramics with varying alumina (Al_2O_3) content levels (0.03, 0.06, and 0.09 wt%) using a bond-based peridynamics. Simulations were conducted using the Large-scale Atomic/Molecular Massively Parallel Simulator (*LAMMPS*) in two stages: equilibrium and impact analysis at velocities of 2, 3, 4, 5, and 6 mm/s. The results showed that with increasing Al_2O_3 content, the crack length also increased, reaching 26.72% at 0.09 wt% Al_2O_3. The reason was attributed to the increase in interparticle repulsion, which led to a decrease in plastic deformation and a decrease in mechanical strength. In addition, the total energy of the system in the 3Y-TZP + 0.03 wt% Al_2O_3 sample decreased by 74.75%.

Cite this article as: Moradkhani A, Hoseinpour Gollo M. Computational fracture analysis of 3Y-TZP dental ceramics with low Al_2O_3 using peridynamics. Sigma J Eng Nat Sci 2026;44(1):375–387.

INTRODUCTION

The increasing demand for durable and biocompatible materials such as yttrium-stabilized tetragonal zirconia polycrystal (3Y-TZP) in dentistry has led to significant advances in the development of ceramic materials. 3Y-TZP has attracted much attention due to its unique mechanical properties, such as high strength, fracture toughness, and fracture resistance [1–3]. These properties make it an ideal choice for use in veneers, bridges, and implants [4,5]. The performance of these materials can be further enhanced by the addition of additives such as aluminum oxide (Al_2O_3), which increases their mechanical behavior and fracture toughness [6–8].

In recent years, the addition of small amounts of Al_2O_3 to 3Y-TZP ceramics has been studied to improve their mechanical properties and increase their reliability in clinical applications. The interaction of 3Y-TZP and Al_2O_3 is of great importance for the overall performance of dental materials. Some studies emphasize the importance of ceramic coatings, such as Al_2O_3, for the mechanical properties of dental ceramics [7, 8]. Kumar et al. [9] showed that a lower Al_2O_3 content can influence heat dissipation and crack propagation in ceramic materials and potentially lead to increased durability [10].

Numerical methods offer a cost-effective way to investigate fracture behavior and mechanisms. The finite element method (FEM) is frequently used to predict brittle fracture,

*Corresponding author.
*E-mail address: m.hoseinpour@sru.ac.ir

This paper was recommended for publication in revised form by Editor-in-Chief Ahmet Selim Dalkilic

crack propagation, and branching [11]. Based on classical continuum mechanics, FEM requires precise tracking of the crack area and propagation direction, as well as determination of the stress intensity factor for accurate analysis. However, its mesh dependency requires re-meshing after each propagation step, which can complicate the modeling of crack growth. For this purpose, the extended finite element method (XFEM) has been used to include discontinuities such as cracks [12]. XFEM enables mesh-independent crack modeling and leads to more accurate simulations, especially in the interaction of macro- and micro-cracks [13].

Peridynamics (PD), introduced by Silling [14], uses integral-differential equations for fracture mechanics and thus allows the investigation of complex crack interactions without tracking the crack tip position. The bond-based PD model effectively predicts crack initiation, propagation, and interactions between primary cracks and microcracks [15–20]. However, due to limitations in the definition of material properties, the state-based PD method was developed, which considers the variable Poisson's ratio in 2-D and 3-D models to achieve more natural results [21]. Simulations using PD are useful for investigating crack growth in brittle materials in that they capture complex interactions between cracks and materials without predefined solutions [22–24].

The peridynamic material point method (PMPM) is a breakthrough in traditional continuum mechanics by simulating crack propagation and material failure without generating an explicit mesh. PMPM has a non-local approach and defines interactions between material points over a finite distance, facilitating the modeling of discontinuities and complex failure behavior [25]. This approach is useful for brittle materials, such as dental ceramics, where crack initiation and growth are of great importance and significantly affect mechanical performance and durability [26]. Complex interactions in heterogeneous materials can be captured by integrating PD and point material methods (PMPM) and investigating the effect of different additives, such as Al_2O_3, on dynamic failure. PMPM is used to improve failure mechanisms for optimization in dental ceramics and improve clinical performance.

Zhou and Qian [27] presented an improved peridynamic model for simulating fractures in composite laminates, validated it using finite element results, and demonstrated its effectiveness in analyzing damage processes. Parkash et al. [28] introduced a bond-based peridynamic model for simulating ceramic impact. It incorporated brittle fracture, plasticity, and strain rate effects, thus enabling fracture analysis. A bond force algorithm facilitated the simulation. Experimental validation showed good agreement in damage prediction. The strain rate-dependent model outperformed existing methods. Chu et al. [29] developed a bond-based peridynamic model for simulating ceramic impact that incorporates brittle fracture, plasticity, and strain rate effects. A bond force algorithm is used to perform the simulation process, and experimental validation has shown good agreement in damage prediction, outperforming the non-ordinary state-based method. Mitts et al. [24] Peridynamic theory (PD theory) was used to predict crack deflection in rotationally symmetric ceramic matrix composites (CMCs). The weak PD equations were used to directly apply the boundary conditions. The study showed that the ratio of critical stress to fracture toughness between coating and matrix significantly influences crack deflection. Smaller ratios lead to earlier deflection in the fiber coating. Lu et al. [30] investigated the dynamic fracture of polycrystalline ice using a peridynamic model. Finite element method (FEM) validation showed that the microstructure significantly influences fracture when grain boundaries are weak, but not when grain boundaries are strong. This study shows that PD is suitable for analyzing fractures in polycrystalline materials and applies it to how cracks propagate in 3Y-TZP + x wt% Al_2O_3 dental ceramics.

Optimization of material composition is essential for improving performance in clinical applications. Computational modeling plays an important role in simulating crack growth. Techniques such as genetic algorithms can optimize these simulations [31–35], while control point algorithms improve reliability by enabling error correction [36, 37]. Efficient load distribution methods further increase computational efficiency in complex analyses [38–40]. Integrating computational methods provides a better understanding of how cracks propagate, and researchers can improve the structural integrity of dental ceramics.

This present study analyzes crack propagation using peridynamic material point simulations in 3Y-TZP + x wt% Al_2O_3 (x = 0.03, 0.06, and 0.09 wt%). The effects of loading conditions, material properties, and Al_2O_3 additive on the fracture behavior of the 3Y-TZP ceramic, as well as on crack initiation and propagation, are systematically investigated. The results contribute to the understanding of the dynamic fracture and failure behavior of 3Y-TZP ceramic and to the development of more durable dental materials.

PD DETAILS

Researchers can precisely model the structural changes of 3Y-TZP ceramics and thus gain valuable insights into how changes in material composition affect crack formation and propagation. The equation of motion [42] is used to illustrate the temporal evolution of the system in each simulation time step based on bond-based peridynamics.

$$\rho(x)\,\ddot{u}(x,t) = \int_H f\left(u(x',t) - u(x,t), x' - x, x\right) dV_{x'} + b(x,t) \tag{1}$$

The equation analyzes forces within a neighborhood (H) of a point x taking into account the displacement vector field (u) and a given volume force density field (b). It also accounts for the mass density (ρ) and a pairwise force function (t) that defines the force exerted on particle x by

another particle x'. ξ is the initial position of the two particles, and η their relative displacement:

$$\xi = x' - x \tag{2}$$

$$\eta = u(x',t) - u(x,t) \tag{3}$$

Figure 1 illustrates how each material point is characterized by the position vector x, engaging in direct interactions with neighboring material points x' through bonds within the defined horizon zone H_x.

According to Newton's third law, there is a theoretical constraint on the force field f as follows [41]:

$$f(x' - x, u' - u, x) = -f(x - x', u - u', x') \tag{4}$$

where the force vector exerted by x on x' is equal in magnitude but opposite in direction to the force vector exerted by x' on x, for any x, x', u, and u'. The principle of angular momentum dictates that the force f must be oriented along the vector that connects deformed shape of x and x'.

$$f(x' - x, u' - u, x) \times ((x' + u') - (x + u)) = 0 \tag{5}$$

A pairwise interaction model is represented by a plot of $|f|$ against bond elongation (ε), defined as follows [41]:

$$\left|(x' + u') - (x + u)\right| - \left|x' - x\right| = \varepsilon \tag{6}$$

The choice of interaction potentials in particle-based simulations is critical as it has a significant influence on the generated data. In this study, the peridynamic prototype micro-elastic brittle "*peri/pmb*" force field [42] is employed to simulate three samples of 3Y-TZP + x wt% Al_2O_3 (x = 0.03, 0.06, and 0.09) dental ceramics. After implementing the standard configurations outlined in Table 1 and the designated force field to the dental ceramics, PD approach was utilized. The simulations were conducted using the Large-scale Atomic/Molecular Massively Parallel Simulator *(LAMMPS)* (2 Aug. 2023 version) package to derive the outputs from equations 4 to 6. Rahman et al. [43] can find detailed initial instructions on utilizing *LAMMPS* for PD in the study. Furthermore, the use of periodic boundary conditions in these simulations allowed for the dental ceramic model to be replicated infinitely in all directions [44-46]. In Figure 2 the algorithm can be seen that used for simulation.

Table 1. PD details in this computational study

Parameter	Parameter ratio/setting
Box dimensions	100 × 100 × 100 mm^3
Boundary condition	Periodic boundary condition [46]
Temperature (°C)	25°C
Pressure (atm)	1
Equilibrium time (μs)	1×10^8
Crack growth time (μs)	1×10^7

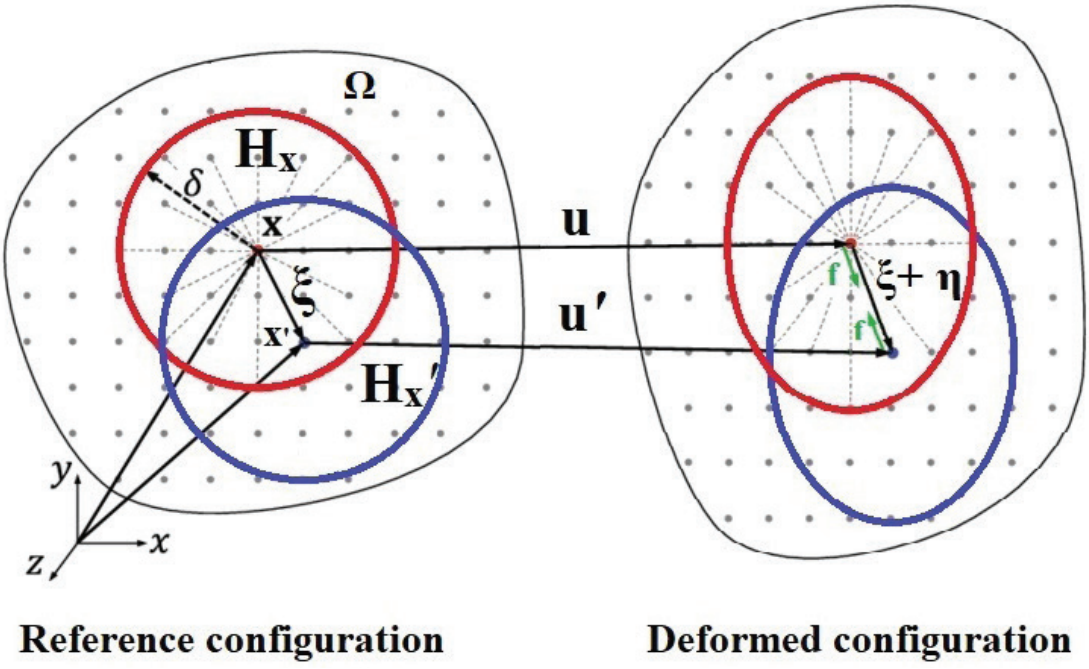

Figure 1. Bond-based peridynamics theory.

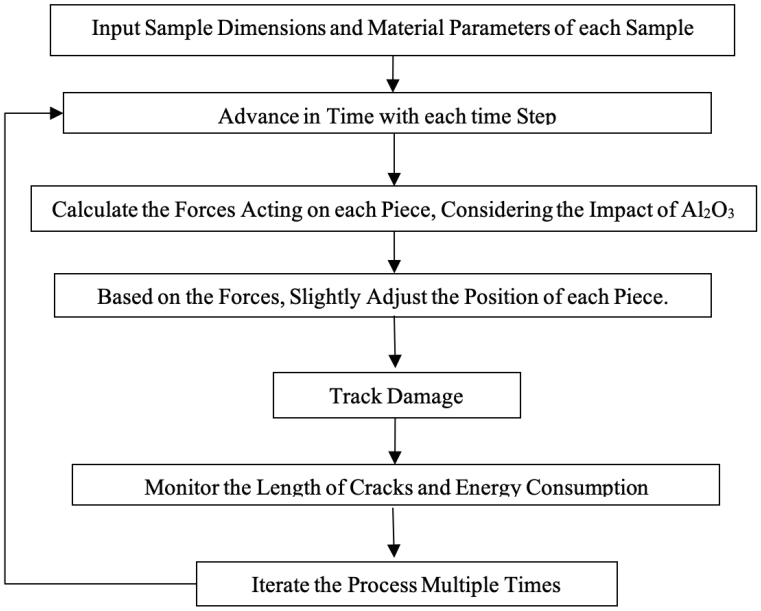

Figure 2. Simulation steps algorithm.

RESULTS AND DISCUSSIONS

Steady-State Simulation

The initial phase consisted of performing the equilibrium process for dental ceramics. Figure 3 presents the particle representation of the pristine 3Y-TZP + x wt% Al_2O_3 dental ceramics beam, created using OVITO (3 Feb. 2021 version) software [48]. The dental ceramics were modeled utilizing the Packmol and Avogadro packages [49, 50]. In addition, Figure 3 highlights the initial notch introduced in the structure, which successfully facilitated crack growth in the following computational step.

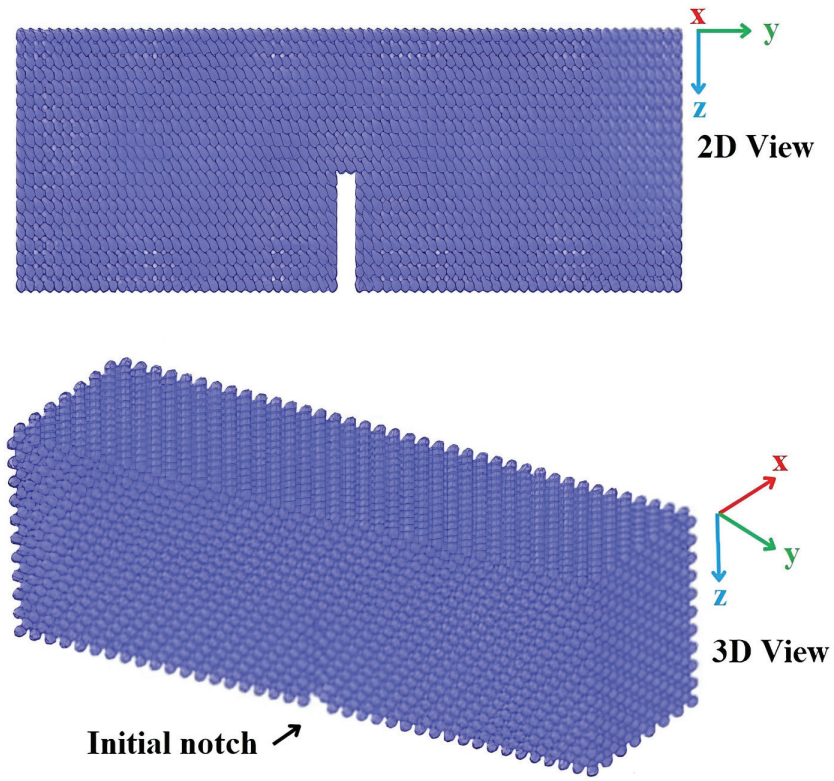

Figure 3. Particle-base structure of 3Y-TZP + x wt% Al_2O_3 dental ceramics beam with initial notch.

The examination of temperature changes in dental ceramics revealed a reduction in the magnitude of particle oscillations over the course of the simulation, as illustrated in Figure 4a. This pattern led to the stabilization of particle movement, converging to a finite ratio and attaining physical stability in the computational model. During the equilibrium phase, PD outputs indicated a decline in particle resonance with each simulation step, leading to a convergence of particle displacement amplitudes to lower values. Consequently, particle mobility stabilized at a constant level. Figure 4b illustrates an examination of the potential energy (PE) curve across three samples, showing a consistent decrease in PE values over time. The curve stabilizes at a fixed function. The negative values in the PE curve indicate a strong attraction between the particles, which maintains their separation throughout the simulation. This approach in the equilibrium phase confirms the validity of the applied methodology and techniques [48, 51, 52].

Table 2. Density changes of pure 3Y-TZP dental ceramics by simulation time steps passing

Time step (μs)	Density (g/cm³)
0	6.119
1×10^7	6.236
2×10^7	6.235
3×10^7	6.008
4×10^7	6.203
5×10^7	6.124
6×10^7	6.142
7×10^7	6.156
8×10^7	6.137
9×10^7	6.126
1×10^8	6.121

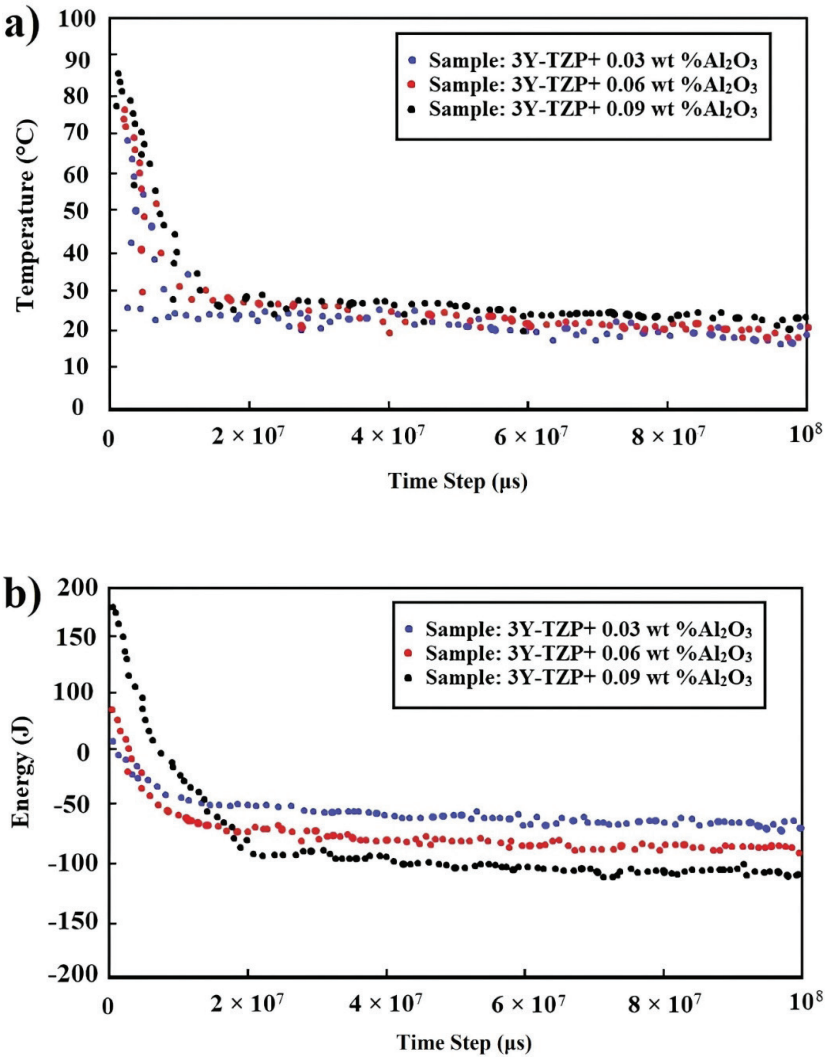

Figure 4. a) Changes in temperature b) Variations in potential energy of 3Y-TZP + wt% Al_2O_3 dental ceramics as per the PD time increments.

To verify the reliability of the calculation methods used, the density changes of the pure 3Y-TZP dental ceramic sample were also investigated. Table 2 indicate that the density stabilized at 6.121 g/cm^3 after 10^8 time steps.

Simulation of Crack Growth

The next phase of the PD study focused on investigating the crack growth mechanism in the 3Y-TZP + wt% Al_2O_3 dental ceramic. At the beginning of this analysis, as shown in Figure 5, a notch was introduced into the unmodified 3Y-TZP matrix. The impact analysis parameters were established within the computational framework, and the initial analysis was conducted at v=2 mm/s according to ASTM 256 [53]. Tracking the extent of cracking in the simulated systems is essential for evaluating the impact response. This variable exhibited a gradual increase over time, with the 3Y-TZP + 0.09 wt% Al_2O_3 showing a more significant rate of progression in contrast to the others. The crack length varied between 7.11 and 9.01 mm, particularly for different dental ceramics, as shown in Figure 6. This result suggests that with increasing Al_2O_3 content, the structural integrity of the sample decreases, leading to lower resistance to external forces and longer cracks.

The stability of the dental ceramic with a pre-crack/initial notch is evident during the crack growth process. The sample's behavior upon fracture initiation is due to the careful simulation parameters and the establishment of specific initial conditions, consistent with earlier studies [7, 24]. Moradkhani et al. [7] investigated the effect of Al2O3 addition on the mechanical properties, dynamic

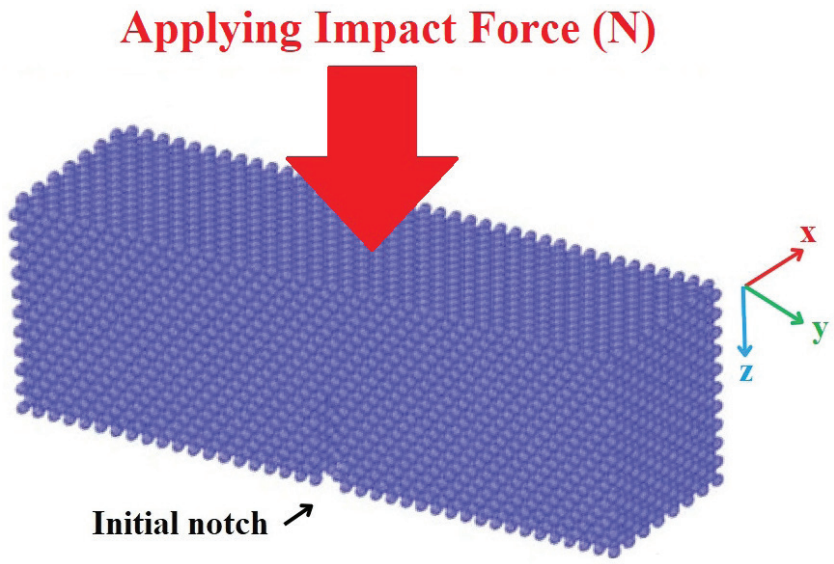

Figure 5. The configuration for the impact during the second stage of PD.

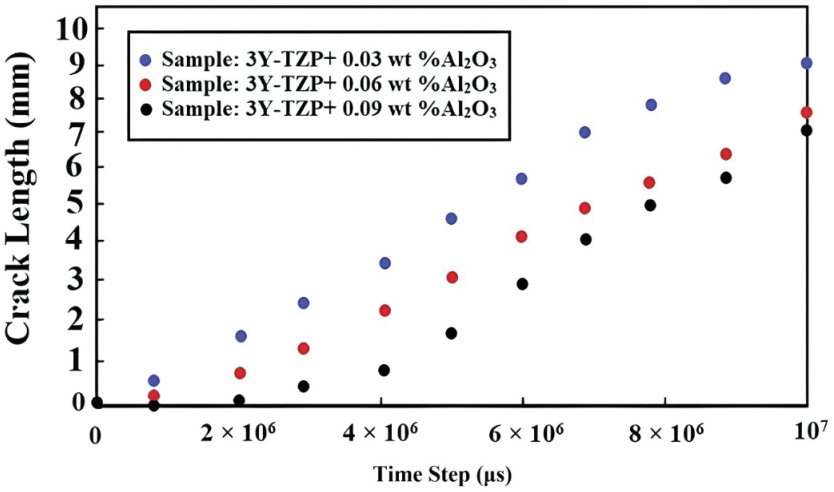

Figure 6. Changes of crack length of 3Y-TZP + x wt% Al_2O_3 dental ceramics.

fracture behavior and strength of 3Y-TZP. Three-point bending test was performed using dental specimens, and the results showed that the highest strength, including 355 MPa, and the best mechanical properties were obtained with 0.05 wt% Al_2O_3. However, stress concentration due to possible cracking can lead to brittle failure [42]. Jing et al. [8] experimentally showed that 3Y-TZP with 0-0.25 wt% Al_2O_3 exhibited high hardness (12.93 GPa) and fracture toughness (9.17 MPa√m), and that hydrothermal stability increased with Al_2O_3 content, and the optimal aging resistance is achieved at 0.15 wt% Al_2O_3. Platt et al. [54] found, using peridynamic simulations in Abaqus, that tensile stress promotes the tetragonal monoclinic phase transformation to zirconia, leading to cracking and reduced confinement of the transforming grain. Aza-Gnandji and Baser [55] investigated the dynamic behavior of differently saturated, frozen soils using bond-based peridynamic and LAMMPS methods. They observed damage failure caused by impact loading and evaluated the effects of projectile size, velocity, and angle on the damage parameters. Rashmehkarim et al. [56] modeled dynamic crack growth using peridynamics in LAMMPS, validated the results, and investigated the influence of stress and pre-crack configuration on crack propagation and branching.

To gain a deeper insight into the crack phenomenon, the highest force exerted on dental ceramic samples was measured. Figure 7 illustrates that the sample 3Y-TZP + 0.09 wt% Al_2O_3 exhibited the highest maximum force among the dental ceramics. This led to a significant influence on the particle distance in various areas of 3Y-TZP + 0.09 wt% Al_2O_3 during the impact analysis, resulting in a reduction of the particle distance and the occurrence of repulsive forces between different components of the dental ceramic. Molecular dynamics simulations indicated an increase in repulsive forces between particles with higher Al_2O_3 additives. Table 3 shows a notable increase at the peak ratio of repulsive force observed at the conclusion of the simulation, from 1.56 N in 3Y-TZP + 0.03 wt% Al_2O_3 to 2.31 N in 3Y-TZP + 0.09 wt% Al_2O_3.

The variations in relative bond lengths were linked to changes in particle arrangement within the samples, significantly influencing the system's energy. Theoretically, there is a reciprocal relationship between PE and relative bond length. This parameter and PE contribute to crack growth, leading to increased crack length. As shown in Figure 8, the relative bond lengths were measured at 0.11, 0.13, and 0.14 mm for 3Y-TZP + x wt% Al_2O_3 (x = 0.03, 0.06, and 0.09), respectively. The structural distinctions led to variations in PE, ranging from 23.62 to 39.01 J across different dental

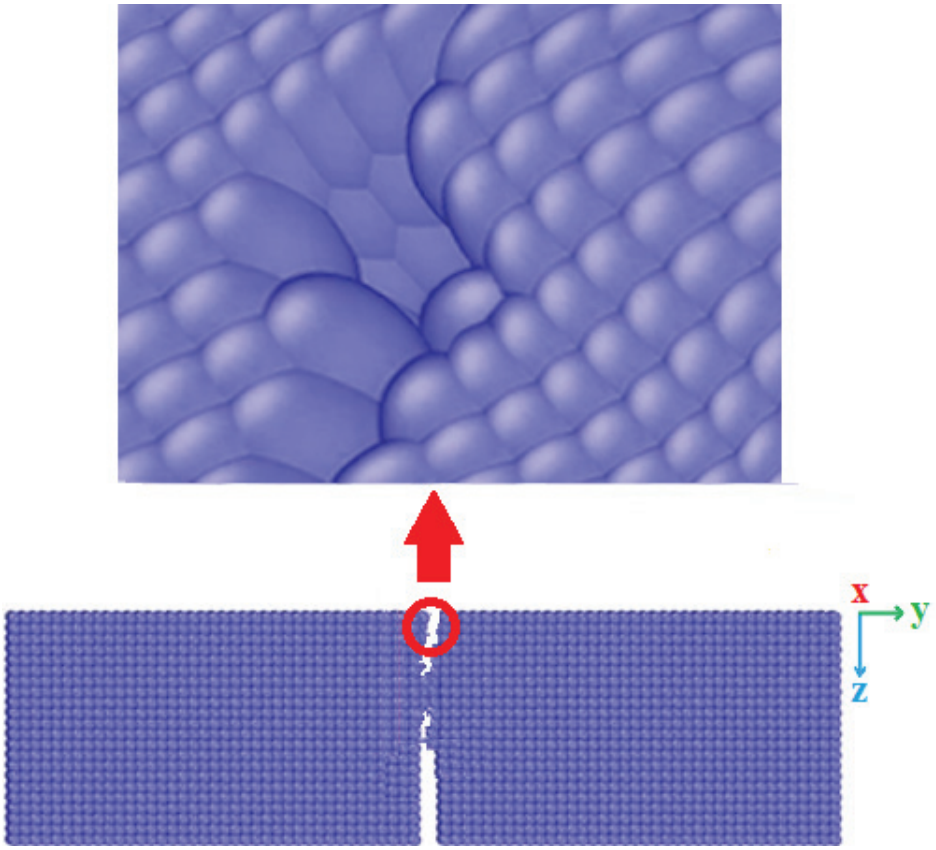

Figure 7. The particle configuration of 3Y-TZP + 0.09 wt% Al_2O_3 dental ceramics following the ımpact analysis conducted at v=2 mm/s.

Table 3. Maximum force (N) and repulsive force (N) ratio values at different time steps in the 3Y-TZP + x wt% Al_2O_3 dental ceramics

Time step (μs)	3Y-TZP+ 0.03 wt %Al_2O_3		3Y-TZP+ 0.06 wt %Al_2O_3		3Y-TZP+ 0.09 wt %Al_2O_3	
	Maximum force (N)	Repulsive force (N)	Maximum force (N)	Repulsive force (N)	Maximum force (N)	Repulsive force (N)
0	0	0	0	0	0	0
1×10^7	1.41	0.32	1.55	0.42	1.73	0.56
2×10^7	1.52	0.54	1.73	0.63	1.92	0.72
3×10^7	1.91	0.61	2.35	0.71	2.68	0.91
4×10^7	3.42	0.76	3.91	0.85	4.56	1.05
5×10^7	3.54	0.92	4.06	1.11	4.89	1.34
6×10^7	4.23	1.04	4.42	1.25	6.34	1.56
7×10^7	4.34	1.26	4.68	1.48	6.95	1.62
8×10^7	6.06	1.33	6.73	1.54	8.23	1.75
9×10^7	6.17	1.57	6.91	1.89	9.75	2.02
1×10^8	6.18	1.56	6.94	2.13	9.76	2.31

ceramics (see Table 4). The effect of PE reduction on particle diffusion was more pronounced in dental ceramics with higher Al_2O_3 content, leading to increased structural deformations and damage. The influence of the reduced PE on particle diffusion was more pronounced in dental ceramics with a higher Al_2O_3 content, leading to increased structural deformations and damage. Simulations of 3Y-TZP + 0.09 wt% Al_2O_3 indicated a culminating damage criterion value of 0.174. The numerical findings obtained in the present stage of PD simulations are summarized in Table 4.

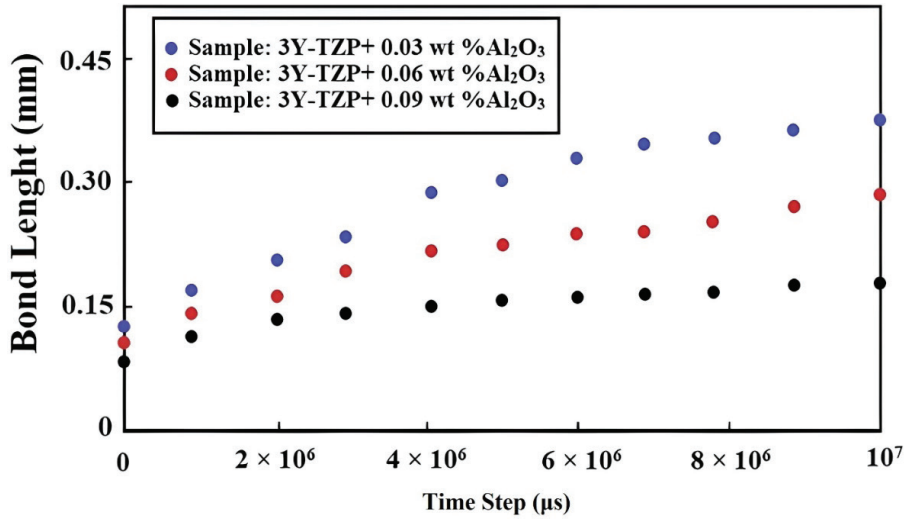

Figure 8. Evolution of relative bond length in modeled 3Y-TZP + x wt% Al_2O_3 over simulation time steps.

Table 4. Characteristics of modeled 3Y-TZP + x wt% Al_2O_3 dental ceramics after 1×10^7 time steps at a velocity of 6 mm/s

3Y-TZP + x wt %Al_2O_3	Crack length (mm)	Net force (N)	Repulsive force (N)	Relative bond length (mm)	Potential energy (J)	Damage criterion
x=0.03	7.11	11.09	2.11	0.15	23.62	0.083
x=0.06	7.94	12.35	2.55	0.26	28.19	0.123
x=0.09	9.01	13.37	2.86	0.37	39.01	0.174

Impact analysis were conducted at 6 mm/s. Figure 9 shows how varying Al_2O_3 content affected crack propagation in the modeled 3Y-TZP + x wt% Al_2O_3 system. Increasing Al_2O_3 increased average particle spacing in the impact zone. This is probably due to the lower mechanical strength in this region resulting from the higher Al_2O_3 content. The simulation results showed that the total force on 3Y-TZP increases with increasing impact fracture velocities. The net force ratio under simulation conditions reached 13.37 N, which increased the displacement of particles in the simulation volume and facilitated crack propagation. Crack growth accelerated with increasing particle displacement in the simulation. Crack lengths at 6 mm/s were 7.11 mm (x=0.03), 7.94 mm (x=0.06), and 9.01 mm (x=0.09). Analysis of repulsive forces showed a value of 2.86 N for the x=0.09 sample at higher velocities.

Table 5 presents the results of six computational calculations. The samples showed significant structural resilience during impact analysis at various speeds. Increased impact velocity correlated with decreased inter-particle distance and reduced mechanical resistance (based on BL and PE analysis).

The data in Table 5 allows for the development of an equation correlating bond length (mm) with velocity for the three samples, as follows:

$$BL_{x=0.03} = 0.0088\,v + 0.1018 \tag{7}$$

$$BL_{x=0.06} = 0.019\,v + 0.1420 \tag{8}$$

$$BL_{x=0.09} = 0.037\,v + 0.1462 \tag{9}$$

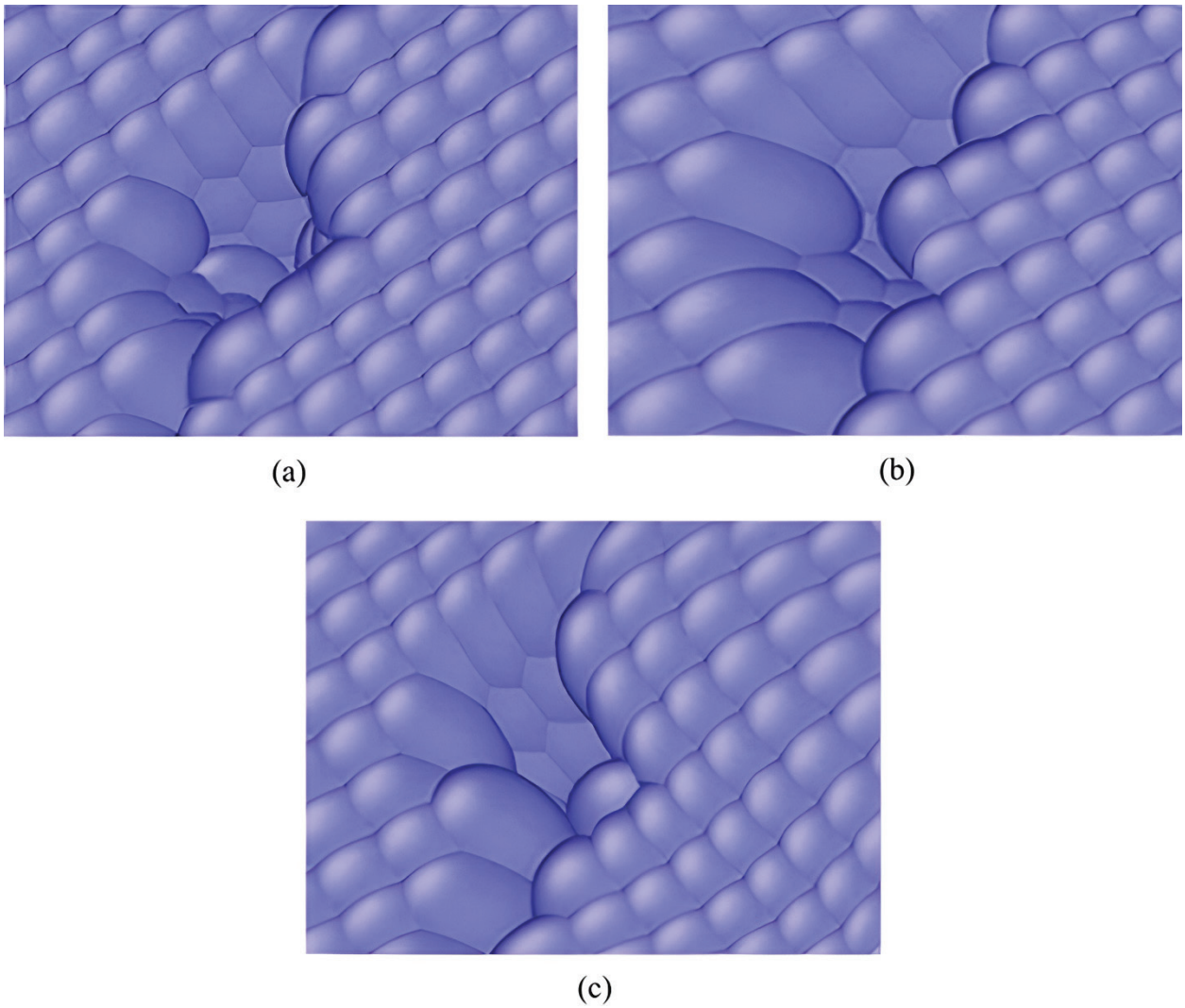

Figure 9. Surface configuration of 3Y-TZP + x wt% Al_2O_3 after impact load at a velocity of 6 mm/s in a) x=0.03, b) x=0.06, c) x=0.09.

Table 5. Effect of impact velocity on 3Y-TZP + x wt% Al_2O_3: crack length, force, and energy parameters

Dental ceramic	3Y-TZP+ 0.03 wt %Al_2O_3					3Y-TZP+ 0.06 wt %Al_2O_3					3Y-TZP+ 0.09 wt %Al_2O_3				
Velocity (mm/s)	2	3	4	5	6	2	3	4	5	6	2	3	4	5	6
Crack length (mm)	7.02	7.07	7.10	7.09	7.11	7.46	7.88	7.91	7.93	7.94	8.85	8.92	8.95	8.97	9.01
Maximum force (N)	6.11	6.14	6.26	6.45	6.55	7.33	7.84	8.03	8.16	8.43	9.65	9.88	10.46	11.37	11.76
Repulsive force (N)	1.55	1.94	1.98	2.07	2.11	2.17	2.19	2.33	2.41	2.55	2.23	2.41	2.56	2.66	2.86
Relative bond length (mm)	0.12	0.13	0.14	0.15	0.15	0.18	0.2	0.21	0.24	0.26	0.22	0.26	0.29	0.33	0.37
Potential energy (J)	22.38	22.69	23.00	23.31	23.62	26.79	27.47	27.49	27.84	28.19	34.62	35.72	36.82	37.92	39.01

Table 6. Potential energy (J) values in brittle material studies

Material	Potential Energy (J)	Reference
3Y-TZP- Al_2O_3	98.42	This study
PMMA composites	67.5	[51]
BNT-Based ceramic	149	[58]
96% Al_2O_3	43.2	[59]
97.7% Al_2O_3	50.6	[59]
Multilayer ceramic capacitors	~200	[60]
$BiFeO_3$-based ceramics	~120	[61]
BNT-based lead-free dielectric ceramics	58	[62]

where v is the test velocity. As the distance between the particles decreased, the attractive forces transformed into repulsive forces (Pauli exclusion principle), which was reflected in changes in potential energy. Using the PD method, potential energy values of 23.62 J (x = 0.03), 28.19 J (x = 0.06), and 39.01 J (x = 0.09) were determined for higher velocities (Table 5). The following equations can express the relationship between PE and velocity:

$$PE_{x=0.03} = 0.31v + 21.758 \quad (10)$$

$$PE_{x=0.06} = 0.35v + 26.09 \quad (11)$$

$$PE_{x=0.09} = 1.098v + 32.428 \quad (12)$$

Increased porosity, resulting from the addition of 0.09 wt% Al_2O_3 to 3Y-TZP, lowered the structural resilience of the dental ceramics, increasing susceptibility to fracture [7]. This suggests that controlling the mechanical strength and operational adaptability of these ceramics is possible by adjusting the Al_2O_3 weight ratio. Akhlaghi-Fard et al. [51] demonstrated, using peridynamics within LAMMPS, that increasing hydroxyapatite in polymethyl methacrylate/hydroxyapatite composites leads to longer cracks. Similarly, in this work, it was found that increasing Al_2O_3 in 3Y-TZP ceramics increases crack length due to interparticle repulsion and decreases total energy. This highlights the influence of composition on crack behavior as modeled by peridynamics. Table 6 compares the potential energy results with other ceramics. Some of the values listed for potential energy in the table are calculated using the following equation [57]:

$$PE = \frac{K^2_{IC}}{E} \times 1000 \quad (13)$$

where K_{IC} is fracture toughness (MPa√m) and E is Young's modulus (GPa).

CONCLUSION

This study examined the fracture behavior of 3 mol% yttria-stabilized tetragonal zirconia polycrystal dental ceramics with varying low alumina content (0.03, 0.06, and 0.09 wt%) using peridynamics simulations. Impact analyses were conducted at velocities of 2, 3, 4, 5, and 6 mm/s. The simulations employed the Peridynamic Material Point Method to model particle interactions in two stages: equilibrium and impact. The outcomes of the peridynamics simulations were as follows:

- The total energy of the 3Y-TZP + x wt% Al_2O_3 dental ceramics system at x=0.03, 0.06, and 0.09 wt% converged to-56.32, -73.22, and -98.42 J, respectively. These

findings suggest an increase in the attractive force between particles within the simulated dental ceramics as the Al_2O_3 ratio decreases.

- The crack length of the simulated dental ceramics reached 9.01 mm at 0.09 wt% Al_2O_3, indicating that an increase in the wt% of Al_2O_3 in the 3Y-TZP leads to a more brittle specimen with reduced mechanical properties.
- Considering the total energy and crack length, 0.03 wt% Al_2O_3 offers a balance. The higher total energy suggests sufficient bonding, while the shorter crack length indicates improved crack resistance. Therefore, a formulation with approximately 0.03 wt% Al_2O_3 is anticipated to exhibit improved mechanical performance for dental restorations.

AUTHORSHIP CONTRIBUTION

All the authors equally contributed to this work.

DATA AVAILABILITY STATEMENT

The authors confirm that the data that supports the findings of this study are available within the article. Raw data that support the finding of this study are available from the corresponding author, upon reasonable request.

CONFLICT OF INTEREST

The author declared no potential conflicts of interest with respect to the research, authorship, and/or publication of this article.

ETHICS

There are no ethical issues with the publication of this manuscript.

STATEMENT ON THE USE OF ARTIFICIAL INTELLIGENCE

Artificial intelligence was not used in the preparation of the article.

REFERENCES

[1] García-de-Albeniz N, Jiménez-Piqué E, Roa JJ, Mas-Moruno C. A review of surface topographical modification strategies of 3Y-TZP: Effect in the physicochemical properties, microstructure, mechanical reliability, and biological response. J EurCeram 2023;43:2977–3004. [CrossRef]

[2] Huang B, Chen M, Wan J, Zhang X. Advances in zirconia-based dental materials: Properties, classification, applications, and future prospects. J Dent 2024;147:105111. [CrossRef]

[3] Muhetaer A, Tang C, Anniwaer A, Yang H, Huang C. Advances in ceramics for tooth repair: From bench to chairside. J Dent 2024;105053. [CrossRef]

[4] Cesar PF, Miranda RBP, Santos KF, Scherrer SS, Zhang Y. Recent advances in dental zirconia: 15 years of material and processing evolution. Dental Mater 2024;40:824–836. [CrossRef]

[5] Upadhyay A, Pradhan L, Yenurkar D, Kumar K, Mukherjee S. Advancement in ceramic biomaterials for dental implants. Int J Appl Ceram Technol 2024;21:2796–2817. [CrossRef]

[6] Moradkhani AR, Baharvandi HR, Vafaeesefat A, Tajdari M. Microstructure and mechanical properties of Al_2O_3-SiC nanocomposites with 0.05% MgO and different SiC volume fraction. ADMT 2012;59:99–105.

[7] Moradkhani A, Gollo MH, Panahizadeh V. Effect of Microstructural Features and Al_2O_3 Doping on Aging Resistance, Mechanical Properties and Crack Propagation in 3Y-TZP Plate Ceramics for Dental Restorations: A Comprehensive Peridynamics Study. Mech Adv Compos Struct 2025;12:523–554.

[8] Jing Q, Bao J, Ruan F, Song X, An S, Zhang Y, et al. High-fracture toughness and aging-resistance of 3Y-TZP ceramics with a low Al Al_2O_3 content for dental applications. Ceram Int 2019;45:6066–6073. [CrossRef]

[9] Kumar KS, Kalos PS, Akhtar MN, Shaik S, Sundara V, Fayaz H, et al. Experimental and theoretical analysis of exhaust manifold by uncoated and coated ceramics (Al_2O_3, TiO_2 and ZrO_2). Case Stud Therm Eng 2023;50:103465. [CrossRef]

[10] Bishnoi D. Pressure exertion and heat dissipation analysis on uncoated and ceramic (Al_2O_3, TiO_2 and ZrO_2) coated braking pads. Mater Today Proc 2023;74:774–787. [CrossRef]

[11] Ganesh KV, Islam MRI, Patra PK, Travis KP. A pseudo-spring based SPH framework for studying fatigue crack propagation. Int J Fatigue 2022;162:106986. [CrossRef]

[12] Belytschko T, Liu WK, Moran B, Elkhodary K. Nonlinear finite elements for continua and structures. New York: John Wiley & Sons; 2014.

[13] Wang H, Liu Z, Xu D, Zeng Q, Zhuang Z. Extended finite element method analysis for shielding and amplification effect of a main crack interacted with a group of nearby parallel microcracks. Int J Damage Mech 2016;25:4–25. [CrossRef]

[14] Dorduncu M, Ren H, Zhuang X, Silling S, Madenci E, Rabczuk T. A review of peridynamic theory and nonlocal operators along with their computer implementations. Comput Struct 2024;299:107395. [CrossRef]

[15] Silling SA, Weckner O, Askari E, Bobaru F. Crack nucleation in a peridynamic solid. Int J Fract 2010;162:219–227. [CrossRef]

[16] Huang D, Lu G, Qiao P. An improved peridynamic approach for quasi-static elastic deformation and brittle fracture analysis. Int J Mech Sci 2015;94:111–122. [CrossRef]
[17] Ha YD, Bobaru F. Characteristics of dynamic brittle fracture captured with peridynamics. Eng Fract Mech 2011;78:1156–1168. [CrossRef]
[18] Bobaru F, Hu W. The meaning, selection, and use of the peridynamic horizon and its relation to crack branching in brittle materials. Int J Fract 2012;176:215–222. [CrossRef]
[19] Basoglu MF, Zerin Z, Kefal A, Oterkus E. A computational model of peridynamic theory for deflecting behavior of crack propagation with micro-cracks. Comput Mater Sci 2019;162:33–46. [CrossRef]
[20] Vazic B, Wang H, Diyaroglu C, Oterkus S, Oterkus E. Dynamic propagation of a macrocrack interacting with parallel small cracks. AIMS Mater Sci 2017;4:118–136. [CrossRef]
[21] Silling SA, Epton M, Weckner O, Xu J, Askari E. Peridynamic states and constitutive modeling. J Elast 2007;88:151–184. [CrossRef]
[22] Silling SA. Reformulation of elasticity theory for discontinuities and long-range forces. J Mech Phys Solids 2000;48:175–209. [CrossRef]
[23] Ha YD, Bobaru F. Studies of dynamic crack propagation and crack branching with peridynamics. Springer 2010;229–244. [CrossRef]
[24] Mitts C, Naboulsi S, Przybyla C, Madenci E. Axisymmetric peridynamic analysis for simulation of crack deflection in ceramic matrix composit. AIAA Scitech 2020;964. [CrossRef]
[25] Zeng Z, Zhang H, Zhang X, Liu Y, Chen Z. An adaptive peridynamics material point method for dynamic fracture problem. Comput Meth Appl Mech Eng 2022;393:114786. [CrossRef]
[26] Bagherzadeh H, Barani OR. Coupling the material point method and Peridynamics via the force partitioning and concurrent coupling schemes. Comput Particle Mech 2024;11:55–71. [CrossRef]
[27] Zhou J, Qian S. Crack propagation simulation of fiber-reinforced composite laminates based on non-ordinary state-based peridynamics. Mater Res Express 2025;12:045501. [CrossRef]
[28] Prakash N, Deng B, Stewart RJ, Smith CM, Harris JT. Investigation of microscale fracture mechanisms in glass–ceramics using peridynamics simulations. J American Ceram Soc 2022;105:4304–4320. [CrossRef]
[29] Chu B, Liu Q, Liu L, Lai X, Mei H. A rate-dependent peridynamic model for the dynamic behavior of ceramic materials. Comput Model Eng Sci 2020;124:151–178. [CrossRef]
[30] Lu W, Li M, Vazic B, Oterkus S, Oterkus E, Wang Q. Peridynamic modelling of fracture in polycrystalline ice. J Mech 2020;36:223–234. [CrossRef]
[31] Rathore NK, Pande S. IoE-based genetic algorithms and their requisition. CRC Press 2023;25–50. [CrossRef]
[32] Rathore NK, Chana I. Checkpointing algorithm in Alchemi. J Inf Technol 2010;8:32–38.
[33] Rathore NK, Khan F. Internet of things: A review article. J Cloud Comput 2018;5:20.
[34] Rathore NK. GridSim installation and implementation process. J Cloud Comput 2015;2:29–40. [CrossRef]
[35] Rathore N. A Review towards: load balancing techniques. J Power Syst Eng 2016;4:47. [CrossRef]
[36] Rathore N. Checkpointing: fault tolerance mechanism. J Cloud Comput 2017;4:28. [CrossRef]
[37] Rathore NK. Installation of Alchemi .NET in computational grid. J Comput Sci 2016;4:1–5. [CrossRef]
[38] Rathore N, Singh PK. A comparative analysis of fuzzy based load balacino algorithms. J J Comput Sci 2017;5:23–33. [CrossRef]
[39] Rathore N. Dynamic threshold based load balancing algorithms. Wirel Pers 2016;91:151–185. [CrossRef]
[40] Rathore NK, Chana I. Comparative analysis of checkpointing. In: Gupta C, Jaroliya D, (editör). IT Enabled Practices and Emerging Management Paradigm. Excel Books 2008. p. 321–327.
[41] Dimitrienko YI. Nonlinear continuum mechanics and large inelastic deformations. New York: Springer; 2010. p. 174. [CrossRef]
[42] Parks ML, Lehoucq RB, Plimpton SJ, Silling SA. Implementing peridynamics within a molecular dynamics code. Comput Phys Commun 2008;179:777–783. [CrossRef]
[43] Rahman R, Foster JT, Plimpton SJ. PDLAMMPS-made easy. University of Texas at San Antonio SNL 2014.
[44] Brown WM, Wang P, Plimpton SJ, Tharrington AN. Implementing molecular dynamics on hybrid high performance computers–short range forces. Comput Phys Commun 2011;182:898–911. [CrossRef]
[45] Plimpton S. Fast parallel algorithms for short-range molecular dynamics. J Comput Phys 1995;117:1–19. [CrossRef]
[46] Plimpton SJ, Thompson AP. Computational aspects of many-body potentials. MRS bulletin 2012;37:513–521. [CrossRef]
[47] Kuzkin VA. On angular momentum balance for particle systems with periodic boundary conditions. ZAMM Z fur Angew Math Mech 2015;95:1290–1295. [CrossRef]
[48] Stukowski A. Visualization and analysis of atomistic simulation data with OVITO–the Open Visualization Tool. Model Simul Mater Sci Eng 2009;18:015012. [CrossRef]
[49] Hanwell MD, Curtis DE, Lonie DC, Vandermeersch T, Zurek E, Hutchison GR. Avogadro: an advanced semantic chemical editor, visualization, and analysis platform. J Cheminf 2012;4:1–17. [CrossRef]

[50] Martínez L, Andrade R, Birgin EG, Martínez JM. PACKMOL: A package for building initial configurations for molecular dynamics simulations. J Comput Chem 2009;30(13):2157–2164. [CrossRef]

[51] Akhlaghi-Fard S, Safari KH, Mashhadi MM, Kheirikhah MM. The computational study of crack growth process in defected polymethyl methacrylate/hydroxyapatite composite beam: peridynamic simulation. Physica Scripta 2023;98(9):095959. [CrossRef]

[52] Akhlaghi-Fard S, Safari HK, Mashhadi MM. 2024. Peridynamic assessment of mechanical and thermal characteristics of a defected PMMA/HA composite beam. J Appl Polym Sci 2024;141(10):e55062. [CrossRef]

[53] ASTM 256-93a, 1995. Standard Test Methods for Determining the Pendulum Impact Resistance of Notched Specimens of Plastics," Annual Book of ASTM Standards, Vol. 08(01)

[54] Platt P. Mella R. DeMaio W, Preuss M, Wenman MR. Peridynamic simulations of the tetragonal to monoclinic phase transformation in zirconium dioxide. Comput Mater Sci2017;140:322–333. [CrossRef]

[55] Aza-Gnandji CD, Baser T. Peridynamic Modeling of Impact Loading in Frozen Soils for In Situ Resource Utilization in the Arctic. Geo-EnvironMeet 2025;128–138. [CrossRef]

[56] Rashmehkarim R, Jafari M, Heidari M. Crack propagation modeling in two-dimensional isotropic plate using bond-based peridynamic theory. J Civ Eng Struct 2025;9.

[57] Li FZ, Shih CF, Needleman A. A comparison of methods for calculating energy release rates. Eng Fract Mech 1985;21:405–421. [CrossRef]

[58] Wang S, Qian J, Ge G, Zhang F, Yan F, Lin J, et al. Embedding Plate-Like pyrochlore in perovskite phase to enhance energy storage performance of BNT-based ceramic capacitors. Adv Energy Mater 2025;15:2403926. [CrossRef]

[59] Rice RW. Grain size and porosity dependence of ceramic fracture energy and toughness at 22 C. J Mater Sci 1996;31:1969–1983. [CrossRef]

[60] Li D, Liu Z, Zhao W, Guo Y, Wang Z, Xu D, et al. Global-optimized energy storage performance in multilayer ferroelectric ceramic capacitors. Nature Commun 2025;16:188. [CrossRef]

[61] Zhou Z, Bai W, Liu N, Zhang W, Chen S, Wang P, et al. Ultrahigh capacitive energy storage of $BiFeO_3$-based ceramics through multi-oriented nanodomain construction. Nature Commun 2025;16:2075. [CrossRef]

[62] Dinh TH, Tran VDN, Le Manh T, Lee JS. Effects of $BaZrO_3$ on the phase evolution and energy storage capacities of BNT-based lead-free dielectric ceramics. J Phys Chem Solids 2025;198:112462. [CrossRef]